Title

Exclusion of alternative exon 33 of CaV1.2 calcium channels in heart is proarrhythmogenic.

Journal

Proceedings of the National Academy of Sciences, 114(21)

Authors

Li, Guang

Wang, Juejin

Liao, Ping

et al.

Publication Date

2017-05-23

DOI

10.1073/pnas.1617205114

Peer reviewed

Exclusion of alternative exon 33 of $Ca_V1.2$ calcium channels in heart is proarrhythmogenic

Guang Li[a,b,1], Juejin Wang[a,c,1], Ping Liao[d], Peter Bartels[a], Hengyu Zhang[a], Dejie Yu[a], Mui Cheng Liang[a], Kian Keong Poh[e], Chye Yun Yu[d], Fengli Jiang[a], Tan Fong Yong[a], Yuk Peng Wong[a], Zhenyu Hu[a], Hua Huang[a], Guangqin Zhang[f], Mary Joyce Galupo[e], Jin-Song Bian[g], Sathivel Ponniah[h], Scott Lee Trasti[i], Kelvin See[j], Roger Foo[j], Uta C. Hoppe[k], Stefan Herzig[l,m], and Tuck Wah Soong[a,d,n,o,2]

[a]Department of Physiology, National University of Singapore, 117597 Singapore; [b]Key Laboratory of Medical Electrophysiology, Ministry of Education, Institute of Cardiovascular Research, Southwest Medical University, Sichuan, 646000 China; [c]Department of Physiology, Nanjing Medical University, Nanjing, 211166 China; [d]National Neuroscience Institute, 308433 Singapore; [e]Department of Medicine, National University of Singapore, 119228 Singapore; [f]Department of Clinical Pharmacy, China Pharmaceutical University, Nanjing, 210009 China; [g]Department of Pharmacology, National University of Singapore, 117600 Singapore; [h]Biological Resource Centre, Agency for Science, Technology and Research, 138668 Singapore; [i]Comparative Medicine, National University of Singapore, 117601 Singapore; [j]Genome Institute of Singapore, 138672 Singapore; [k]Department of Internal Medicine II, Paracelsus Medical University, Salzburg, 5020 Austria; [l]Center of Molecular Medicine, University of Cologne, Cologne, 50931 Germany; [m]Department of Pharmacology, University of Cologne, Cologne, 50931 Germany; [n]Graduate School for Integrative Sciences and Engineering, National University of Singapore, 117456 Singapore; and [o]Neurobiology/Ageing Programme, National University of Singapore, 117456 Singapore

Edited by Kurt G. Beam, University of Colorado Denver, Aurora, CO, and approved April 18, 2017 (received for review October 17, 2016)

Alternative splicing changes the $Ca_V1.2$ calcium channel electrophysiological property, but the in vivo significance of such altered channel function is lacking. Structure–function studies of heterologously expressed $Ca_V1.2$ channels could not recapitulate channel function in the native milieu of the cardiomyocyte. To address this gap in knowledge, we investigated the role of alternative exon 33 of the $Ca_V1.2$ calcium channel in heart function. Exclusion of exon 33 in $Ca_V1.2$ channels has been reported to shift the activation potential −10.4 mV to the hyperpolarized direction, and increased expression of $Ca_V1.2_{\Delta 33}$ channels was observed in rat myocardial infarcted hearts. However, how a change in $Ca_V1.2$ channel electrophysiological property, due to alternative splicing, might affect cardiac function in vivo is unknown. To address these questions, we generated m*Cacna1c* exon $33^{-/-}$-null mice. These mice contained $Ca_V1.2_{\Delta 33}$ channels with a gain-of-function that included conduction of larger currents that reflects a shift in voltage dependence and a modest increase in single-channel open probability. This altered channel property underscored the development of ventricular arrhythmia, which is reflected in significantly more deaths of exon $33^{-/-}$ mice from β-adrenergic stimulation. In vivo telemetric recordings also confirmed increased frequencies in premature ventricular contractions, tachycardia, and lengthened QT interval. Taken together, the significant decrease or absence of exon 33-containing $Ca_V1.2$ channels is potentially proarrhythmic in the heart. Of clinical relevance, human ischemic and dilated cardiomyopathy hearts showed increased inclusion of exon 33. However, the possible role that inclusion of exon 33 in $Ca_V1.2$ channels may play in the pathogenesis of human heart failure remains unclear.

CaV1.2 channel | alternative splicing | cardiac function | cardiac arrhythmia | heart failure

The L-type $Ca_V1.2$ calcium channels are critically important for the initiation of muscle contraction. Structural variations of $Ca_V1.2$ channels generated via alternative splicing diversify channel electrophysiological properties to optimize their function (1, 2). Inclusion of cassette exon 33 shifts the activation potential of the $Ca_V1.2$ channel, and this variant will require larger depolarization of membrane potential to open. Notably, exon 33 is regulated developmentally, and its expression is altered by pathology such as myocardial infarction (2–4).

Structure–function studies have been performed of $Ca_V1.2$ channels heterologously expressed in cell lines or in isolated cardiomyocytes, but results from these in vitro experiments may not inform in vivo relevance (5, 6). The major reason is because it is almost impossible to reconstitute a native in vivo milieu in cell lines that have heterologously expressed a defined combination of the subunits that compose the $Ca_V1.2$ channel complex. The electrophysiological properties of the $Ca_V1.2$ channels can be diversified by the association with one of four β-subunits or one of four α2δ-subunits. To further expand the range of diversification, each of the subunits could be alternatively spliced and posttranslationally modified. As such, at best, one could make predictions from in vitro results of in vivo significance; however, work done on the $Ca_V1.2$ channels has not produced such results, and there are still many controversies and contradicting published data (5, 6).

To directly address in vivo significance of altered $Ca_V1.2$ channel property arising from alternative splicing, we have generated exon-specific knockout mice deleting alternative exon 33 of the L-type $Ca_V1.2$ channel. Questions have been asked about the importance that a modest voltage-dependent change in electrophysiological properties of ion channels has on physiology. In this study, we show dramatic effects on cardiac function arising from a voltage shift in activation potential of the $Ca_V1.2_{\Delta 33}$ channels. The hearts of the exon 33-null (exon $33^{-/-}$)

Significance

To directly address in vivo significance of the altered $Ca_V1.2$ channel property arising from alternative splicing, we generated $Ca_V1.2$ exon 33-specific knockout (exon $33^{-/-}$) mice. Here, we showed that the exclusion of alternative exon 33 altered $Ca_V1.2$ biophysical property, leading to greater I_{Ca} density. This increase in current density induced prolongation of ventricular cardiomyocyte action potential duration, and the cardiomyocytes exhibited increased early afterdepolarizations and autonomous action potentials—hallmarks of arrhythmias. In vivo, exon $33^{-/-}$ mice had increased occurrences of premature ventricular contractions, tachycardia, and lengthened QT interval. As such, exclusion of exon 33 of the $Ca_V1.2$ channel is proarrhythmogenic. Although failing human hearts had greater inclusion of exon 33, it is unclear whether the inclusion is compensatory, neutral, or damaging.

Author contributions: G.L., J.W., P.L., S.H., and T.W.S. designed research; G.L., J.W., P.L., P.B., H.Z., D.Y., M.C.L., C.Y.Y., F.J., T.F.Y., Y.P.W., Z.H., H.H., M.J.G., S.P., and S.L.T. performed research; K.K.P., G.Z., J.-S.B., S.P., K.S., R.F., U.C.H., and T.W.S. contributed new reagents/analytic tools; G.L., J.W., P.L., P.B., H.Z., D.Y., M.C.L., K.K.P., C.Y.Y., F.J., T.F.Y., Y.P.W., Z.H., H.H., G.Z., M.J.G., J.-S.B., S.L.T., S.H., and T.W.S. analyzed data; and G.L., J.W., P.L., and T.W.S. wrote the paper.

The authors declare no conflict of interest.

This article is a PNAS Direct Submission.

[1]G.L. and J.W. contributed equally to this work.

[2]To whom correspondence should be addressed. Email: phsstw@nus.edu.sg.

This article contains supporting information online at www.pnas.org/lookup/suppl/doi:10.1073/pnas.1617205114/-/DCSupplemental.

mice were found to develop ventricular arrhythmias. Whereas echocardiographic and pressure–volume measurements showed increased contractility, in vivo telemetric recordings showed increased frequency in premature ventricular contractions and spontaneous ventricular tachycardia. The underpinning mechanisms for these cardiac defects are larger current densities of the $Ca_V1.2_{\Delta 33}$ channels due to a left-shift of activation potential, a modest increase in single-channel open probability (Po), and a shorter closed time.

Results

Exon $33^{-/-}$ Cardiomyocytes Have a Similar Surface Expression of $Ca_V1.2$ Channels. Exon $33^{-/-}$ mice were generated by cre-mediated genetic targeting (7) to remove exon 33 from the m*Cacna1c* gene (Fig. 1*A* and *SI Appendix*, Fig. S1*A*). The mice were genotyped as WT ($^{+/+}$), heterozygous ($^{+/-}$), and homozygous ($^{-/-}$) by the predicted restriction-enzyme fragments of 10.0 kb for WT (+) and 8.0 kb for null (−) alleles (Fig. 1*B*). To examine the exon 33 deletion in the m*Cacna1c* transcripts, we used RT-PCR to detect a 351-bp PCR product for WT, a 318-bp PCR product for null, and 351- and 318-bp products for heterozygotes (Fig. 1*C*), and these results were confirmed by DNA sequencing (*SI Appendix*, Fig. S1*B*).

Genetic deletion of exon 33 also did not alter the $Ca_V1.2$ transcript levels as examined by real-time PCR of mRNAs isolated from the left ventricles (*SI Appendix*, Fig. S1*C*). Of note, immunolabeling with pan-$Ca_V1.2$ antibody revealed typical striation patterns in isolated cardiomyocytes (*SI Appendix*, Fig. S1*D*) without obvious signs of hypertrophy at 6 mo. Importantly, the total protein of $Ca_V1.2$ in whole heart (*SI Appendix*, Fig. S1*E*) and the surface expression level of $Ca_V1.2$ in isolated cardiomyocytes (Fig. 1 *D* and *E*) was unaltered, providing assurance that deletion of exon 33 did not alter surface expression of the $Ca_V1.2$ channels.

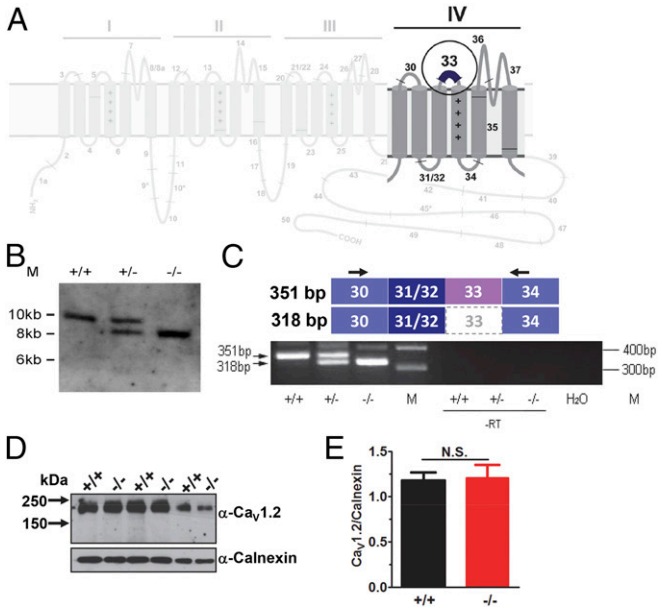

Fig. 1. Characterization of exon $33^{-/-}$ mice. (*A*) Schematic diagram showing the topology of the $Ca_V1.2$ α1 subunit. It consists of four domains (I–IV), and each domain comprises six transmembrane segments. Domain IV is highlighted in dark gray, and the position of exon 33 is indicated as a blue bar, highlighted within a circle, between the DIVS3-S4 loop. (*B*) Southern blot analyses of WT and exon $33^{-/-}$ genomic DNAs. The NsiI restriction-enzyme digestions generated WT (exon $33^{+/+}$, 10 kb) and targeted (exon $33^{-/-}$, 8 kb) hybridizing bands. (*C*) RT-PCR analysis of left ventricle mRNA. The PCR products of predicated sizes (exon $33^{+/+}$: 351 bp and exon $33^{-/-}$: 318 bp) were detected. (*D*) Surface expression of $Ca_V1.2$ channels on isolated ventricular cardiomyocytes from WT ($n = 3$) and exon $33^{-/-}$ ($n = 3$) mice. Antibodies against the α1-subunit of $Ca_V1.2$ channels were used to detect surface expression of $Ca_V1.2$ channels, and anti-calnexin antibody was used for normalization of membrane proteins. (*E*) Normalized $Ca_V1.2$ channel protein levels of WT and exon $33^{-/-}$ cardiomyocytes were analyzed by a two-tailed unpaired *t* test ($P = 0.863$).

To ascertain that genetic targeting of exon 33 did not affect other alternative splicing events, we used restriction enzyme digestions and/or amplicon sizes of RT-PCR products to determine levels of expression of alternative exons. The major alternative exons of transcript-scanned m*Cacna1c* were found to be unchanged in expressions except that mutually exclusive exon 32 was expressed at a higher level in exon $33^{-/-}$ hearts (*SI Appendix*, Fig. S2). However, we have shown previously that the inclusion of mutually exclusive exon 31 or 32 did not change the electrophysiological properties of the $Ca_V1.2$ channels (2, 8). To further analyze the combinatorial splicing patterns in the exon $33^{-/-}$ mice, we generated a pool of full-length $Ca_V1.2$ cDNAs (9), and, using appropriate pairs of primers, we colony-screened to detect the inclusion and exclusion of nine alternative exons of each cDNA clone expressed in *Escherichia coli*. Our results showed that the splicing combinations of the cardiac $Ca_V1.2$ channels remained similar, except for the loss of exon 33 and the higher expression of exon 32 over exon 31 (*SI Appendix*, Table S1).

As our objective was to assess cardiac function, we measured the protein levels of known ion channels required for the generation of the ventricular action potentials (APs) and found that their expression levels were similar (*SI Appendix*, Fig. S3*A*). Moreover, the hearts of WT and exon $33^{-/-}$ mice were morphologically similar with no obvious signs of hypertrophy at 6 mo of age (*SI Appendix*, Fig. S3 *B–E*). To evaluate global transcript expressions between WT and exon $33^{-/-}$ hearts, our microarray experiments did not show any significant changes in transcripts that are important in Ca^{2+} homeostasis (*SI Appendix*, Tables S6–S8). No significant differences were detected for calcium channel $\alpha_2\delta$- or β-subunits or for protein phosphatases (*SI Appendix*, Tables S9–S11). These combined data suggest that any changes in cardiac AP property would be due largely to the altered characteristics of Ca^{2+} current (I_{Ca}) fluxing through the $Ca_V1.2_{\Delta 33}$ channels (10).

Exon $33^{-/-}$ $Ca_V1.2$ Currents in Cardiomyocytes Are Larger. To determine the underlying mechanism for the phenotypes in the exon $33^{-/-}$ hearts, we performed electrophysiological recordings in isolated cardiomyocytes and found that the current density was increased by 33% (Fig. 2 *A* and *B*) and that the steady-state activation and inactivation potentials of I_{Ca} were left-shifted (Fig. 2 *C* and *D*). This gave rise to a calcium window-current that peaks at −24 mV for exon $33^{-/-}$ mice, which is 12 mV more hyperpolarized than WT (Fig. 2*D*). The larger electrochemical force for the $Ca_V1.2_{\Delta 33}$ channels accounted for the larger current density recorded in exon $33^{-/-}$ cardiomyocytes (1.99 pA/pF). The half-activation potential ($V_{0.5}$) was also left-shifted by 10.1 mV, suggesting that the $Ca_V1.2_{\Delta 33}$ channels were more easily opened upon depolarization from rest (Fig. 2*B*); however, the rate of recovery from inactivation was similar (*SI Appendix*, Fig. S4 *A* and *B*). However, the ventricular AP-triggered calcium currents, as recorded in whole-cell voltage-clamp mode, were nonetheless 60% larger in the exon $33^{-/-}$ cardiomyocytes (Fig. 2 *E* and *F*).

Exon $33^{-/-}$ $Ca_V1.2$ Single Channels Have a Modest Increase in Open Probability. The increase in current density in the exon $33^{-/-}$ cardiomyocytes could be explained by an increase in surface expression, which we had earlier excluded; a shift in voltage dependence, which we have shown in Fig. 2 and previously reported for $Ca_V1.1$ channels (11); or a modest increase in maximum Po of the $Ca_V1.2_{\Delta 33}$ channels (12, 13). Single-channel recordings showed increased channel activity in the exon $33^{-/-}$ cardiomyocytes at +10 mV (Fig. 2*G*) and over several test potentials (*SI Appendix*, Fig. S4*C*), which also indicated a modest

increase in maximum Po. The increase in Po could be explained by a shorter time in channel activation (mean first latency), a longer channel open time (mean open time), and a shorter channel closed time (mean closed time) (*SI Appendix*, Table S2).

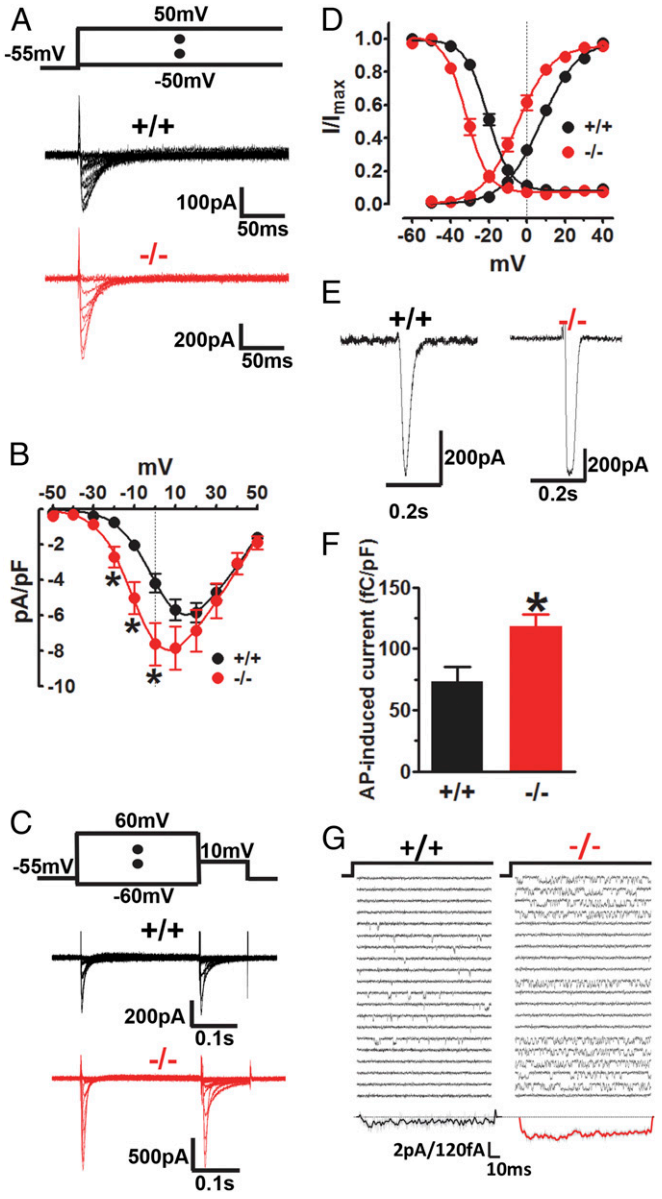

Fig. 2. Larger I_{Ca} in exon $33^{-/-}$ cardiomyocytes. (*A* and *B*) Current–voltage relationship of $Ca_V1.2$ channels in WT (n = 11 cells, $V_{0.5}$ = −1.58 ± 2.3 mV) and exon $33^{-/-}$ (n = 18 cells, $V_{0.5}$ = −11.68 ± 3.3 mV) cardiomyocytes (*P < 0.05 vs. WT, unpaired t test). (*C* and *D*) Steady-state activation and inactivation properties of $Ca_V1.2$ channels in WT (n = 16 cells, $V_{0.5,inact}$ = −25.03 ± 0.44 mV) and exon $33^{-/-}$ (n = 12 cells, $V_{0.5,inact}$ = −36.34 ± 0.64 mV) cardiomyocytes. (*E*) Sample traces of ventricular AP-induced calcium currents recorded in WT and exon $33^{-/-}$ cardiomyocytes. (*F*) Summary of calcium influx induced by AP waveform stimulation (n = 5 cells for WT mice and n = 5 cells for exon $33^{-/-}$ mice; *P < 0.01, unpaired t test). (*G*) Single-channel recordings of $Ca_V1.2$ channels in WT and exon $33^{-/-}$ cardiomyocytes. Twenty consecutive exemplary traces (k = 1 channel) indicate increased basic gating properties of exon $33^{-/-}$ cardiomyocytes. The test potential was +10 mV. Below the graphs are 180 traces (n = 1 cell) from the same experiment averaged to a sum current. The scale bars in pA refer to single-channel events. The sum current is depicted in fA.

Exon $33^{-/-}$ Cardiomyocyte $Ca_V1.2$ Channels Are More Sensitive to Nifedipine, but Show No Differences in Isoproterenol or Forskolin Stimulation. As nifedipine inhibition is state-dependent (14, 15), we determined that the half maximal inhibitory concentration (IC_{50}) for nifedipine inhibition was 10.6 nM for exon $33^{-/-}$ and 22.8 nM for WT cardiomyocytes (Fig. 3*A*), and application of 10 nM nifedipine blocked exon $33^{-/-}$ I_{Ca} by ∼15% more than WT (Fig. 3*B*). These results substantiated the third mechanism that we proposed for nifedipine blockade in which an altered biophysical property of the $Ca_V1.2$ channels due to alternative splicing is associated with sensitivity to blockade by nifedipine (4). The other two mechanisms are due to inclusion of mutually exclusive exon 8 or 8a that encodes the DIS6 segment and the more depolarized resting potential of smooth muscle compared with cardiac muscle. However, the responses to β-adrenergic stimulation were similar between WT and exon $33^{-/-}$ cardiomyocytes, unlike in human heart failure (13) (Fig. 3 *C* and *D*). Application of isoproterenol (ISO) slightly left-shifted *I–V* curves of both WT and exon $33^{-/-}$ $Ca_V1.2$ channels (Fig. 3*E*), but an increase in I_{Ca} was not different for various concentrations of ISO used (Fig. 3*F*). Similarly, use of a range of concentrations of foskolin also resulted in comparable increases of I_{Ca} in WT and exon $33^{-/-}$ cardiomyocytes (Fig. 3*G*).

Exon $33^{-/-}$ Cardiomyocytes Have a Longer Action Potential Duration and Exhibit Increased Early After-Depolarizations and Autonomous Action Potentials. Potentiating the $Ca_V1.2_{\Delta 33}$ channels should prolong ventricular AP (16) by increasing Ca^{2+} influx (Fig. 2 *E* and *F*), and we found that the action potential duration (APD) after 90% repolarization ($APD_{90\%}$) in exon $33^{-/-}$ cardiomyocytes was 66.7% longer than in WT, but $APD_{20\%}$ and $APD_{50\%}$ were unaltered (Fig. 4 *A* and *D*). Application of 100 nM nifedipine reduced the $APD_{90\%}$ in exon $33^{-/-}$ cardiomyocytes significantly but not in WT (Fig. 4 *A* and *E*), suggesting that the repolarizing potassium currents were not affected (17). The resting membrane potential was similar in WT and exon $33^{-/-}$ cardiomyocytes (Fig. 4*B*), although the refractory period in exon $33^{-/-}$ was longer by ∼40% (Fig. 4*C*), which could be attributed to the slower repolarization of the AP.

The occurrence of early after-depolarization (EAD), an indicator of cardiac arrhythmia, which could be mediated by prolonged APD and reactivated Ca^{2+} influx through $Ca_V1.2$ channels (18, 19), was increased by 2.7 times in exon $33^{-/-}$ over WT cardiomyocytes (Fig. 4 *F* and *G*). This result is in agreement with a previous report that showed that generation of EAD was highly sensitive to shifts in activation potential of L-type calcium channels (20). Another indicator of cardiac dysfunction is the generation of autonomous APs after the cessation of electrical stimulation, and again the exon $33^{-/-}$ cardiomyocytes showed increased frequency of 3.4 times over WT (Fig. 4 *H* and *I*), suggesting dysregulation in intracellular calcium (21, 22). Taken together, the irregular excitation of exon $33^{-/-}$ cardiomyocytes was due largely to increased Ca^{2+} influx through the $Ca_V1.2_{\Delta 33}$ channels.

Exon $33^{-/-}$ Hearts Are Prone to Arrhythmia and Increased Cardiac Contractility. To examine in vivo significance, we paced the intact heart electrically with the application of ISO (1 mg/kg, i.p. injection) (23) and detected that exon $33^{-/-}$ hearts were more susceptible to the generation of ventricular tachyarrhythmia (Fig. 5*A*) (24). Half of the exon $33^{-/-}$ mice developed ventricular tachyarrhythmia, whereas none of the WT did (Fig. 5*B*), for a duration of ∼1 s (Fig. 5*C*). Examination of heart function by echocardiography showed no differences in left-ventricular-wall thickness, chamber dimensions, and mass, but there was significantly higher left ventricular ejection fraction (LVEF: 77 ± 6% vs. 73 ± 7%), greater fractional shortening (40 ± 5% vs. 36 ± 6%), and higher cardiac output (CO: 16 ± 4 vs. 13 ± 3 mL/min) in the exon $33^{-/-}$ mice (*SI Appendix*, Fig. S5 and Table S3). Furthermore, we analyzed the pressure–volume (*P–V*) conductance by Millar

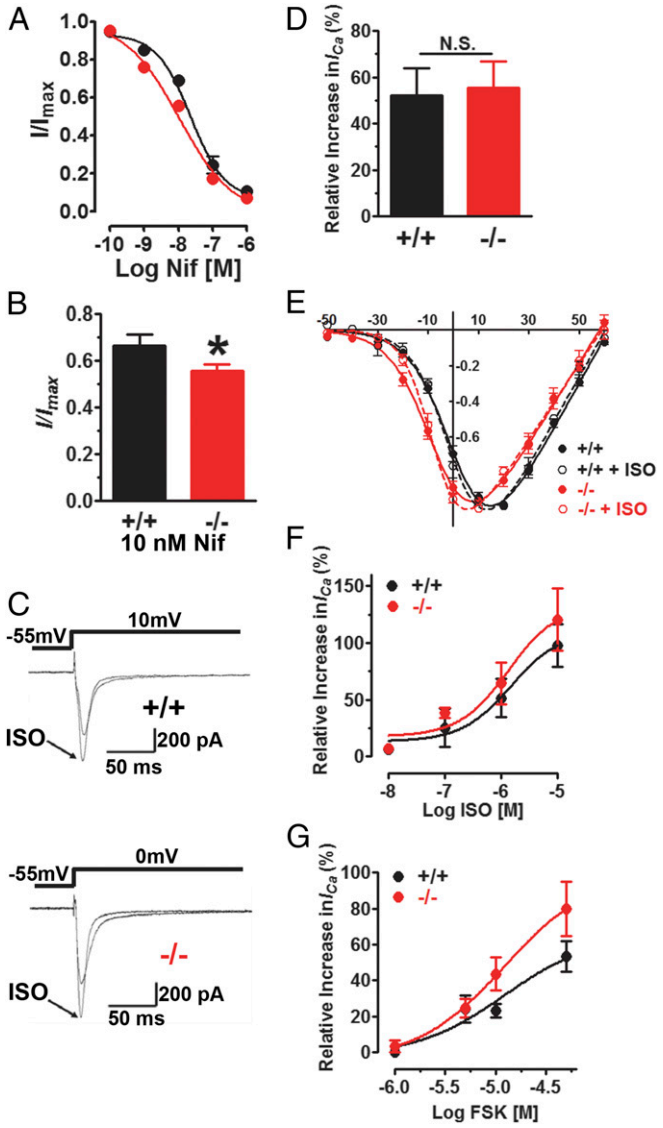

Fig. 3. Exon $33^{-/-}$ cardiomyocytes are more sensitive to nefedipine but have similar responses to β-adrenergic stimulation. (*A*) Response of $Ca_V1.2$ channels in WT ($n = 20$ cells; test pulse: 10 mV) and exon $33^{-/-}$ ($n = 27$ cells; test pulse: 0 mV) cardiomyocytes to nifedipine block (WT: $IC_{50} = 22.8$ nM vs. exon $33^{-/-}$: $IC_{50} = 10.6$ nM; $P < 0.001$, unpaired *t* test). (*B*) Difference in sensitivity of 10 nM nifedipine blockade between WT ($n = 5$ cells) and exon $33^{-/-}$ ($n = 7$ cells) cardiomyocytes (*$P = 0.038$, unpaired *t* test). (*C*) Sample traces of $I_{Ca,L}$ before and after 1 μM ISO application. For WT cardiomyocytes, a +10-mV depolarizing stimulation was applied. For exon $33^{-/-}$ cardiomyocytes, a 0-mV depolarizing pulse was applied to activate the channels to open at peak. (*D*) Summary of effects of ISO on $I_{Ca,L}$ recorded from WT ($n = 13$ cells) and exon $33^{-/-}$ ($n = 12$ cells) cardiomyocytes. ($P = 0.657$, unpaired *t* test). (*E*) Current–voltage relationship (*I–V*) curves were analyzed before and after 1 μM ISO application in WT ($V_{0.5}$: 2.18 ± 0.74 mV; $n = 13$ vs. 0.76 ± 1.08 mV; $n = 4$) and exon $33^{-/-}$ cardiomyocytes ($V_{0.5}$: −5.53 ± 0.89 mV; $n = 15$ vs. −6.8 ± 0.79 mV; $n = 4$). (*F*) Relative increase in $I_{Ca,L}$ upon application of various concentrations of ISO in WT ($n = 8$, $EC_{50} = 1.47$ μM) and exon $33^{-/-}$ cardiomyocytes ($n = 7$; $EC_{50} = 1.33$ μM). (*G*) Relative increase in $I_{Ca,L}$ upon application of various concentrations of forskolin (FSK) in WT ($n = 5$; $EC_{50} = 12.3$ μM) and exon $33^{-/-}$ cardiomyocytes ($n = 6$; $EC_{50} = 12.2$ μM).

catheter, and consistent with echocardiographic measurements, *P–V* loop data indicated that exclusion of exon 33 in $Ca_V1.2$ channels significantly increased cardiac contractility (LVEF: 49 ± 8% vs. 40 ± 7%) and output (CO: 13.8 ± 4.2 vs. 9.1 ± 3.5 mL/min) in the exon $33^{-/-}$ mice compared with WT mice (*SI Appendix*, Table S4).

The enhanced cardiac contractility is correlated with increased electrically induced Ca^{2+} transients (*SI Appendix*, Fig. S6 *A* and *B*) observed in the exon $33^{-/-}$ cardiomyocytes. To further investigate Ca^{2+} handling in these cardiomyocytes, we examined the properties of regional Ca^{2+} sparks in resting cardiomyocytes (*SI Appendix*, Fig. S6*C*). Although the spark amplitude and frequency were similar, there were significant augmentations in spark spatial width (full width at half maximum) and temporal duration (full duration at half maximum), indicating increased elemental Ca^{2+} release (*SI Appendix*, Fig. S6 *D–G*).

In Vivo Telemetric Recordings Detected Increased Premature Ventricular Contractions and Tachycardia, Prolonged QT Interval, Increased Heart Rate, and Increased Contractility in Exon $33^{-/-}$ Mice. To further determine the in vivo consequences of deletion of exon 33, WT and exon $33^{-/-}$ mice were implanted with transmitters and allowed to recover over 7 d before the device was activated for electrocardiogram (ECG) and aortic blood pressure recordings for 12 h from 7 PM to 7 AM. The exon $33^{-/-}$ hearts exhibited a three- to fourfold increase in the appearance of premature ventricular contractions (Fig. 5 *D* and *E*), whereas ∼30% of exon $33^{-/-}$ mice showed spontaneous ventricular tachycardia (Fig. 5 *D* and *F*) compared with none for WT littermates. The QT interval for the exon $33^{-/-}$ mice was ∼73% longer than for the WT mice (Fig. 5 *G* and *H*), whereas the heart rate was slightly higher (Fig. 5*I*). Overall, the in vivo consequence of the altered $Ca_V1.2$ channel property owing to the absence of alternative exon 33 was proarrhythmogenic. The QA interval, which is an indicator of contractility, was lower in exon $33^{-/-}$ mice (Fig. 5 *J* and *K*), also suggesting that exon $33^{-/-}$ hearts have an increased contractility.

Increased Death Rate of Exon $33^{-/-}$ Mice After ISO Treatment Over 30 Days. After administering 10 mg/kg/d of ISO over 30 d, exon $33^{-/-}$ mice died at a threefold higher frequency than WT littermates (Fig. 6*A*). The gross morphology of the exon $33^{-/-}$ ISO-treated hearts was much larger and the weight was heavier, but not the heart:body mass ratio (Fig. 6 *B* and *C*). These data clearly demonstrated that the β-adrenergic effect was still intact in the exon $33^{-/-}$ hearts and that activation of the β-adrenergic receptor exacerbated the cardiac electrical phenotype of the exon $33^{-/-}$ mice.

Human Heart Failure Has Significantly Higher Expression of Exon 33. To relate the mouse data with potential clinical relevance, we characterized exon 33 expressions in human nonfailing and failing hearts (*SI Appendix*, Table S5). Single-channel recordings of human nonfailing and failing hearts have been reported (13), and failing cardiomyocytes displayed little change in expression of the $Ca_V1.2$ α_1- or β-subunits but a defect in dephosphorylation. We extracted mRNAs from human hearts, including those previously reported (13), to determine the expression level of $Ca_V1.2$ exon 33 (Fig. 6*D*) and found that in nonfailing heart (Fig. 6 *D* and *E*) the expression level was ∼60%, which is similar to normal adult human heart (2, 4, 9). In contrast, the inclusion of exon 33 increased significantly by ∼20% in human ischemic and dilated cardiomyopathy failing hearts (Fig. 6*D*, *Middle* and *Lower*, and *E*).

Discussion

The difficulty of interpreting in vitro results for in vivo significance is strikingly reflected in the controversies and uncertainties that still exist after 20 y of research on β-adrenergic regulation of the $Ca_V1.2$ channels (5, 6). Clearly, in vitro conditions cannot recapitulate the cellular milieu or physiological context by which $Ca_V1.2$ channels function properly in native cardiomyocytes. To complicate matters, native channel properties could be diversified by posttranscriptional or posttranslational modifications, which again cannot be fully mimicked in in vitro experiments where cloned $Ca_V1.2$ channel subunits are heterologously expressed in cell lines that are of noncardiac origin.

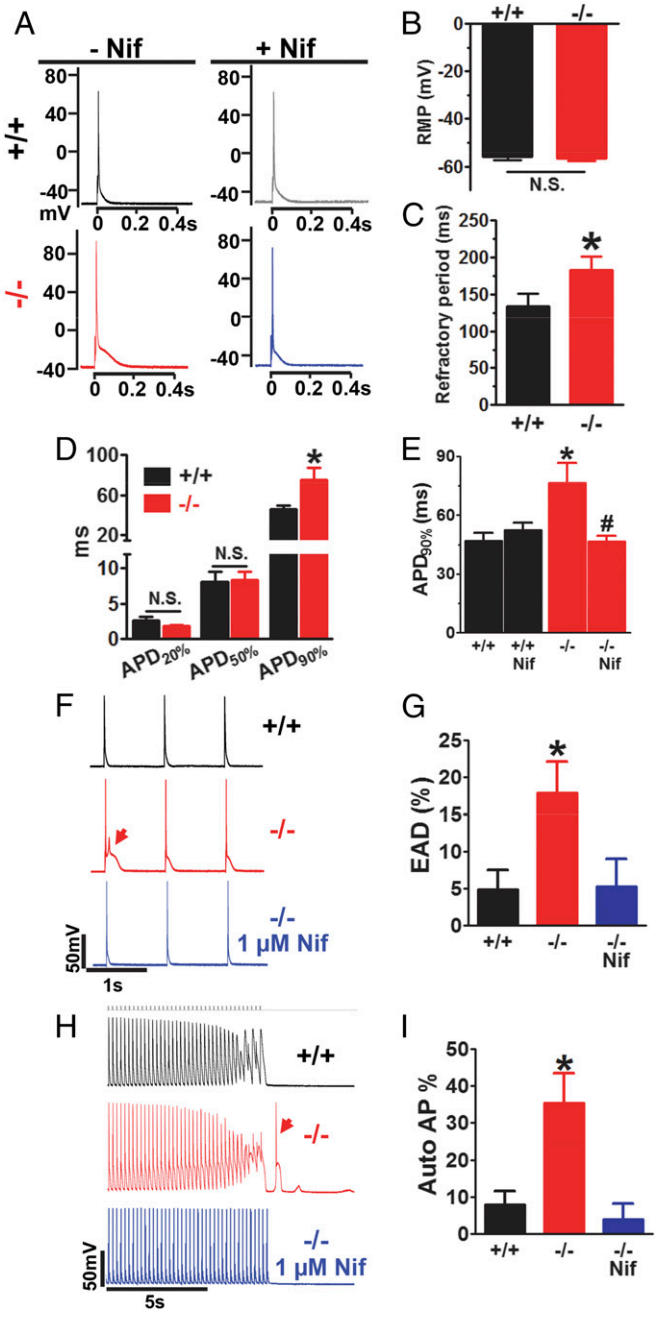

Fig. 4. Prolonged action potential duration and increased frequency of EADs and autonomous action potentials in exon $33^{-/-}$ cardiomyocytes. (*A*) APs recorded from WT and exon $33^{-/-}$ cardiomyocytes before and after 0.1 μM nifedipine application. (*B*) Resting membrane potentials recorded from WT ($n = 10$ cells) and exon $33^{-/-}$ ($n = 15$ cells) cardiomyocytes ($P = 0.766$, unpaired *t* test). (*C*) Refractory periods of APs recorded from WT ($n = 14$ cells) and exon $33^{-/-}$ ($n = 24$ cells) (*$P = 0.0408$, unpaired *t* test). (*D*) Summary of APDs after 20% ($APD_{20\%}$), 50% ($APD_{50\%}$), and 90% of repolarization ($APD_{90\%}$) from WT ($n = 16$ mice) and exon $33^{-/-}$ ($n = 11$ mice) (*$P = 0.0281$ vs. WT, unpaired *t* test). (*E*) $APD_{90\%}$ of exon $33^{-/-}$ cardiomyocytes was reduced to a level similar to WT after application of 0.1 μM nifedipine (WT: $n = 15$ cells; exon $33^{-/-}$: $n = 20$ cells; *$P < 0.05$ vs. WT, one-way ANOVA followed by Bonferroni post hoc test); #$P < 0.05$ vs. exon $33^{-/-}$ cardiomyocytes without nifedipine treatment, unpaired *t* test with Welch's correction. (*F* and *G*) Detection of EAD in cardiomyocytes in WT ($n = 73$ cells, 17 mice), exon $33^{-/-}$ ($n = 73$ cells, 16 mice), and exon $33^{-/-}$ treated with 1 μM nifedipine ($n = 37$ cells, 10 mice) at a 0.5-Hz pacing rate. *$P = 0.0156$, one-way ANOVA followed by Bonferroni post hoc test. (*H* and *I*) Detection of autonomous APs in cardiomyocytes from WT ($n = 73$ cells, 17 mice), exon $33^{-/-}$ ($n = 73$ cells, 16 mice), and exon $33^{-/-}$ treated with 1 μM nifedipine ($n = 22$ cells, 8 mice) at a 5-Hz pacing rate (*$P = 0.0013$, one-way ANOVA followed by Bonferroni post hoc test).

Our work in generating the exon $33^{-/-}$-null mice has provided direct evidence that a shift in cardiac $Ca_V1.2$ channel activation in the hyperpolarized direction has profound effects on native cardiac membrane excitability leading to adverse heart rhythmicity and enhanced muscle contractility. Curiously, the expression of exon 33 of the $Ca_V1.2$ channel is ∼60% in human heart in contrast to ∼90% expression in rodents (2). As such, in humans there is a wider dynamic range for variation in exon 33 expression levels to produce an adaptive, deleterious, or protective effect (inclusion of exon 33), as exon 33-containing $Ca_V1.2$ channels allow reduced Ca^{2+} influx. This notion is supported by the increased inclusion of exon 33 in $Ca_V1.2$ channels found in human failing hearts. The proportion of $Ca_V1.2$ transcripts with exon 33 was increased from ∼60% in nonfailing hearts to ∼80% in failing hearts. A possible interpretation is that increased expression of $Ca_V1.2_{33}$ channels could be a compensatory response to heart failure in humans. In human heart failure, the loss of T-tubules could lead to a remodeling and redistribution of $Ca_V1.2$ channels from the dyadic junctions to the caveolae membrane (25–27) and might contribute to arrhythmogenesis. The inclusion of exon 33 in $Ca_V1.2$ channels as shown by our data is antiarrhythmogenic and would therefore suggest a compensatory effect.

In this report, there are a few unexpected observations that are also of clinical relevance. First, unlike overexpressed $Ca_V1.2$ transgenic murine models where the Po of the channels was either smaller (28) or remained the same (29), our data showed a modest increase in Po, supporting the evidence that increased Po of cardiac $Ca_V1.2$ channels could contribute to failing human hearts, although the previously reported results were due mainly to hyperphosphorylation of the channels (13). Second, a totally unexpected result was the lack of hypertrophy in the 6-mo-old exon $33^{-/-}$ mice. This is in sharp contrast to the $Ca_V1.2$ α_1- or β_2-overexpressed transgenic mice where hypertrophy was observed at 6 mo and the mice died before 12 mo of age from heart failure (30–33). Similar modest Ca^{2+} influx was reported by us and Muth et al. (30), and yet there was a drastic difference in pathology. One explanation could be that nonconducting effects of $Ca_V1.2$ channels may signal to trigger expression of hypertrophy genes (34, 35), or the distribution of Cav1.2 channels to specific domains within the cardiomyocytes may play a role (25, 26). Third, the β-adrenergic effect was not blunted over the range of concentrations of ISO used in our exon $33^{-/-}$ myocytes, unlike what was reported in $Ca_V1.2$ overexpression transgenic mice or in human heart failure. Our microarray results showed that the $Ca_V\beta_2$ subunit or calcineurin (PP2A) transcript levels did not decrease, which may explain the preservation of the β-adrenergic stimulation of $Ca_V1.2$ activity. Interestingly, the coupling efficiency between $Ca_V1.2$ channels and ryanodine receptors (RyRs) may be increased as Ca^{2+} transients and the duration of the Ca^{2+} sparks were larger in exon $33^{-/-}$ cardiomyocytes (29). The exon $33^{-/-}$ mice did not exhibit any of the characteristics of human heart failure such as severe hypertrophy or attenuation of β-adrenergic signaling. Instead, the electrical remodeling of the $Ca_V1.2$ channels contributed more toward cardiac arrhythmia.

In mouse cortical neurons, increased Rbfox1/2 proteins have been shown to developmentally enhance the inclusion of exon 33 in $Ca_V1.2$ channels (36). Therefore, of general interest is the decrease in Rbfox1 expression in human and mouse failing hearts (37), but in our human data, the exon 33 level was increased, and it is possible that Rbfox1 regulation of human exon 33 inclusion is different from mice. However, of specific interest is the possibility of variations or mutations within the Rbfox1 binding site (UGCAUG) (38) that might produce

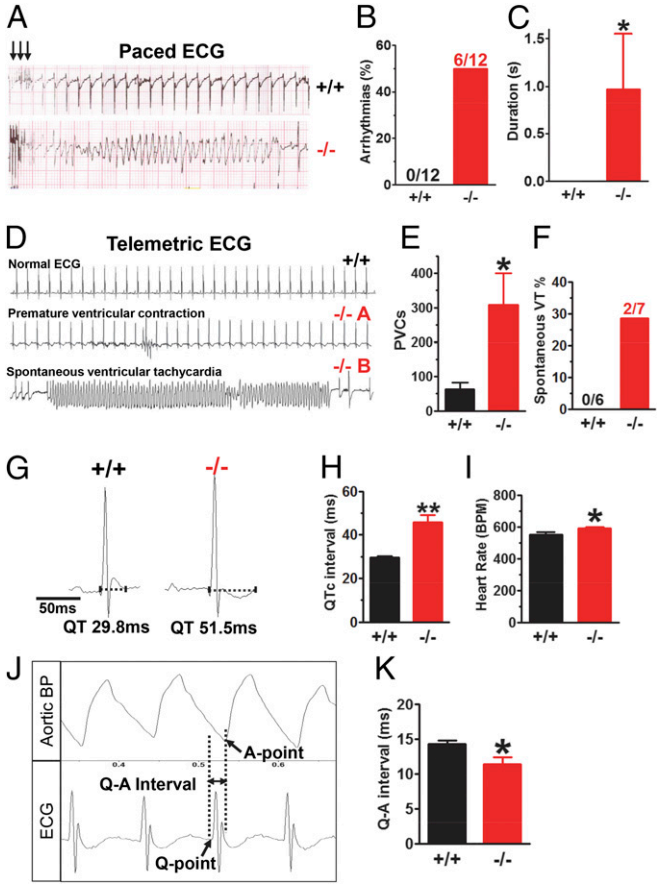

Fig. 5. Increased cardiac arrhythmia and contractility in exon $33^{-/-}$ hearts. (*A*) ECG traces obtained from WT and exon $33^{-/-}$ mice after pacing. (*B*) Number of mice that developed ventricular arrhythmia. (*C*) Averaged duration of ventricular arrhythmia (WT: $n = 6$ mice; exon $33^{-/-}$: $n = 6$ mice; $^*P < 0.01$, unpaired t test). (*D*) Exemplary traces obtained for normal, premature ventricular contractions, and ventricular tachycardia ECGs. (*E*) Premature ventricular contractions (PVCs) of the WT ($n = 6$) or exon $33^{-/-}$ ($n = 7$) mice from 7:00 PM to 7:00 AM were counted ($^*P = 0.0387$, unpaired t test). (*F*) Events of spontaneous ventricular tachycardia (VT) were also counted from 7:00 PM to 7:00 AM. (*G*) Representative ECG waveforms were recorded from WT and exon $33^{-/-}$ mice at 12:00 AM. (*H*) QT intervals of WT ($n = 7$) and exon $33^{-/-}$ ($n = 6$) mice were calculated and corrected for heart rates [QTc = QT/$(RR/100)^{1/2}$; $^{**}P = 0.0044$, unpaired t test]. (*I*) Heart rates were also analyzed in 12-h recordings from WT ($n = 6$) and exon $33^{-/-}$ ($n = 7$) mice; $^*P = 0.0376$, unpaired t test. (*J*) Waveforms were obtained from simultaneous recordings of aortic blood pressure (*Upper* graphs) and ECG (*Lower* graphs). (*K*) The QA intervals from WT ($n = 4$) vs. exon $33^{-/-}$ ($n = 6$) mice were analyzed by unpaired t test; $^*P = 0.0461$.

moderate effects on cardiac function under normal conditions through the modulation of exon 33 inclusion or skipping, but might trigger arrhythmia when stressed.

Ca^{2+} homeostasis in heart failure has been reported to be maintained by a few possible mechanisms, namely a decrease in expression of $Ca_V1.2$ (12), an increase in expression of Na^+/Ca^{2+} exchanger (NCX) (29), or a decrease in expression of the β_2 subunit (28). Here, we show a mechanism where Ca^{2+} homeostasis is influenced by the altered utilization of alternative exon 33 to decrease Ca^{2+} influx and may produce an antiarrhythmogenic effect in human heart failure (13).

The exon $33^{-/-}$-null mice are highly unique as the electrical property of the ventricular AP has been altered with dire consequences. In contrast, cardiac-specific overexpression of $Ca_V1.2$ α_1- or β-subunits by different groups did not yield consistent results in the phenotype characterization of heart failure (28, 30, 33, 39). Although these transgenic mice died from heart failure within 12 mo as a result of hypertrophy, our exon $33^{-/-}$ mice have been maintained and lived past 2 y of age. Our microarray results also showed that the expression levels of the $Ca_V\beta$-subunits, $Ca_V\alpha_2\delta$-subunits, NCX, sarco/endoplasmic reticulum Ca-ATPase, phospholamban, and RyR transcripts remained relatively unchanged, providing strong suggestion that Ca^{2+} handling within the cardiomyocytes was not adversely affected. In summary, it is possible that the gain-of-function of $Ca_V1.2_{\Delta 33}$ channels, when expressed at the crest of ventricular myocytes, contributed to the proarrhythmic triggers, but expression at the T-tubules did not significantly affect coupling to the RyRs to produce hypertrophy (26).

In conclusion, we have provided direct evidence for the in vivo significance of the altered $Ca_V1.2$ channel property due to alternative splicing.

Materials and Methods

Construction of Targeting Vector and Generation of $Ca_V1.2$ Exon $33^{-/-}$ Mice. The SV129 mouse Bacterial Artificial Chromosome (BAC) clones, containing genomic sequences that include the region spanning exon 30 to exon 36 of the $Ca_V1.2$ channel *Cacna1c* gene (National Center for Biotechnology Information: NM_009781.3), were identified from a BAC library (Invitrogen) by PCR, and the clones were DNA-sequenced for confirmation. A ~10.6-kb region containing exon 33 and the flanking intronic sequences was isolated using restriction enzyme NsiI and subcloned into a modified pCR-XL-TOPO vector. The 5′ intron of exon 33 served as the long homology arm, and the 3′ intron of exon 33 served as the short homology arm. The PGK-neo gene cassette served as the positive selection marker of the targeting vector and was ligated with exon 33 (*SI Appendix*, Fig. S1*A*). The exon 33 and neo^R cassette were flanked by the loxP sequences used for subsequent cre-loxP recombination. The targeting vectors were linearized with MluI endonuclease and transfected into SV129 embryonic stem (ES) cells by electroporation. About 300 G418 (250 μg/mL)-resistant clones were screened by PCR, and the desired integrated ES clones were confirmed by Southern blot analysis using an external probe (*SI Appendix*, Fig. S1*A*). The positive ES clones were further electroporated with cre plasmid to delete exon 33 and neo cassette. The resulting G418-sensitive cell clones were expanded for

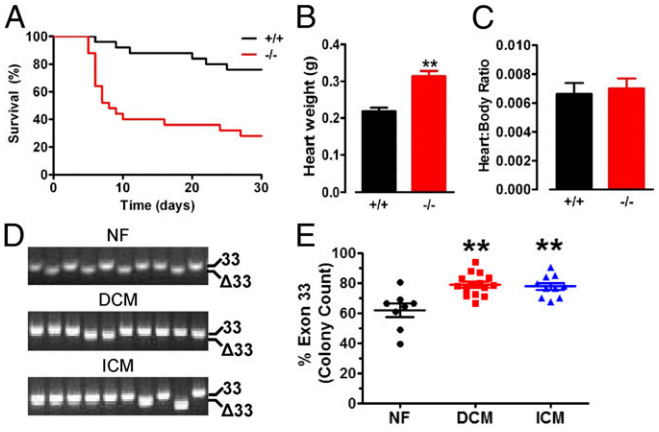

Fig. 6. Increased death of ISO-treated exon $33^{-/-}$ mice and up-regulation of $Ca_V1.2$ exon 33 in failing human hearts. (*A*) Kaplan–Meier plots show survival rates in the WT ($n = 12$) or exon $33^{-/-}$ ($n = 19$) mice after ISO treatment (10 mg/kg/day) and monitored over 30 d; $P = 0.0002$, log-rank test. Analyses of WT ($n = 7$) or exon $33^{-/-}$ ($n = 8$) mice 51 d after ISO treatments (10 mg/kg/day) for heart weight (*B*) and heart:body mass ratio (*C*); $^{**}P < 0.01$, unpaired t test. (*D*) Agarose gel images of PCR products showing inclusion of exon 33 (33: 218 bp) and exclusion of exon 33 (Δ33: 185 bp) after bacterial colony screening of amplicons amplified from mRNAs isolated from human non-failing (NF), ischemic (ICM), or dilated cardiomyopathy (DCM) hearts. (*E*) The combined data for the inclusion of exon 33 in the $Ca_V1.2$ channels of NF ($n = 8$), DCM ($n = 15$), and ICM ($n = 10$); $^{**}P < 0.01$, one-way ANOVA followed by Bonferroni post hoc test.

microinjection into C57BL/6J mice blastocysts. The germline chimeras with agouti color were crossed with C57BL/6J mice into the fourth to fifth generations. Male littermates with the same genetic background were used for experiments. All animals were treated ethically in accordance with the approved institutional animal care and use committee protocol of the National University of Singapore.

Determination of Mouse Genotypes and Analysis of Gene Expression. Southern blot analysis was used to determine the mouse genotypes. The genomic DNA was extracted from tail clipping and digested using restriction enzyme *NsiI* (New England Biolabs). Details are found in *SI Appendix, Supplemental Experimental Procedures*.

Cell-Surface Biotinylation and Western Blotting. Cell-surface proteins from mouse cardiomyocytes were isolated using the Cell Surface Protein Isolation kit (Pierce), following the manufacturer's protocol with minor modification for suspension cells. Details are found in *SI Appendix, Supplemental Experimental Procedures*.

Generation and Analysis of Full-Length Cardiac $Ca_V1.2$ cDNA Clones by PCR. Total RNA was isolated from the left ventricle of one WT and two exon $33^{-/-}$ mice using an RNeasy Kit (QIAGEN). Details are found in *SI Appendix, Supplemental Experimental Procedures*.

Isolation of Single Adult Mouse Cardiomyocytes. Single cardiomyocytes were isolated from male adult mouse heart (2–4 mo). The mice were injected intraperitoneally with 1,000 IU heparin and euthanized in a CO_2 chamber. The heart was immediately transferred to precooled Tyrode solution, and the surrounding tissues (including lung) were removed. The aorta was cannulated using 27G blunted needles and tied using 6.0 surgical threads. Then the heart was mounted onto the Langendorff apparatus and it was perfused through the aorta with prewarmed and oxygenated normal Ca^{2+}-free Tyrode solution for 5 min. Following this procedure, the heart was perfused with the same solution but containing 0.28 mg/mL Protease Type XIV (P5147, Sigma-Aldrich) and 0.84 mg/mL collagenase type I (C0130, Sigma-Aldrich) for more than 8–10 min. The left ventricle tissue was dissected, diced into small pieces with a pair of small scissors, and gently stirred in a petri dish containing the same normal Tyrode solution without enzyme. The dissociated cells were filtered with a stainless steel cell dissociation sieve (S1145, Sigma-Aldrich) and washed three times by centrifugation. Finally, the Ca^{2+} concentration of the Tyrode solution was increased gradually to 1.0 mM in 20 min to maintain the isolated cardiomyocytes in physiological medium (40).

Whole-Cell Electrophysiological Recording. Whole-cell L-type calcium channel current (I_{Ca}) of exon $33^{-/-}$ and WT cardiomyocytes were recorded using the patch clamp technique (41). Details are found in *SI Appendix, Supplemental Experimental Procedures*.

Cell-Attached Single-Channel Recording. Single-channel recordings were carried out in the cell-attached configuration using an Axopatch 200B amplifier (Molecular Devices) as reported previously (42). Details are found in *SI Appendix, Supplemental Experimental Procedures*.

Paced Electrocardiography. In vivo cardiac electrophysiology was carried out as described previously (43, 44). Mice were anesthetized by i.p. injection with pentobarbital sodium (45 mg/kg) and immobilized on a heating pad set to 37 °C. To maintain physiological breathing and avoid an open-chest operation, a paired unipolar electrode was attached to the ventricle through the diaphragm by an abdominal access. The electrode was connected to a stimulator, and a burst pacing protocol (10 pulses with 40-ms intervals and 1.0-ms pulse width) was applied using twice the amount of voltage of the stimulating threshold. The threshold was determined by pacing the heart with increased voltages at a rate 20% higher than the individual mouse heart rate output. Pacing was started 2 min after i.p. injection of ISO (1 mg/kg). The ECG recording started 2 min before ISO injection and continued for 5 more min after injection.

Measurements of Local Ca^{2+} Release Events and $[Ca^{2+}]_i$ Transient. We used a laser-scanning confocal microscope and the fluorescent Ca^{2+} indicator Fluo-4 as reported previously (45) to detect Ca^{2+} sparks in resting cardiomyocytes bathed in normal Tyrode solution. Details are found in *SI Appendix, Supplemental Experimental Procedures*.

Echocardiography. Echocardiography was carried out using a Vivid 7 ultrasound system with a 13-MHz high-frequency linear array transducer (i13L, GE Healthcare). This was performed by sonographers blinded to the genotype of the mice and in groups containing WT and exon $33^{-/-}$ mice. A total of 20 mice in each group were examined. After 2D imaging, the left ventricular systolic and diastolic dimensions in M-mode in the parasternal short axis view were measured at the level of the papillary muscles (46, 47). Fractional shortening, ejection fraction, and mass were calculated from the M-mode parasternal short-axis view (48). Heart rate was derived from pulse wave Doppler profiles at the left ventricular outflow tract. Cardiac output was derived by the cubed method [1.047 × (left ventricular end diastolic diameter^3 – left ventricular end systolic diameter^3) × heart rate] (49).

Pressure–Volume Measurement. Mice were anesthetized with a mixture of ketamine (100 mg/kg i.p. injection) and xylazine (2.5 mg/kg i.p. injection) and maintained by the administration of 0.5–1.0% isoflurane. For physiological closed-chest preparation, the 1.4-Fmicrotip pressure–volume conductance catheter (Millar Instruments) was inserted via the right carotid artery and advanced into the left ventricle of the WT or exon $33^{-/-}$ mouse guided by echocardiography. Left ventricle pressure–volume signals were measured as described previously (50). Data were analyzed using PVAN3.2 software (Millar Instruments).

Expression of Exon 33 in Human Ventricular Heart Samples. Five nonfailing (NF) and 10 failing (F) heart samples were obtained from U.C.H. and 2 nonfailing (NF), 16 failing (F) heart samples were obtained by R.F. from the University of Cambridge, Cambridge, UK, and one normal, pooled human heart cDNA purchased from Clontech Laboratories (Takara Bio USA) were used in this study. Institutional IRB approvals for this study were obtained for U.C.H. (Ethical Committee of the University of Cologne, 9743), for R.F. (Papsworth Hospital Research Tissue bank, project number T02252), and for T.W.S. (National University of Singapore IRB Committee, NUS-IRB 04-086). Details about the samples are found in *SI Appendix, Supplemental Experimental Procedures*.

ACKNOWLEDGMENTS. We thank Dr. Carol Tang and Wei-ping Yu for help in karyotyping of ES cells. This work was supported by grants from the Biomedical Research Council and the National Medical Research Council of Singapore (to T.W.S.).

1. Pitt GS, Dun W, Boyden PA (2006) Remodeled cardiac calcium channels. *J Mol Cell Cardiol* 41:373–388.
2. Tang ZZ, et al. (2004) Transcript scanning reveals novel and extensive splice variations in human l-type voltage-gated calcium channel, Cav1.2 alpha1 subunit. *J Biol Chem* 279:44335–44343.
3. Liao P, et al. (2009) Molecular alteration of Ca(v)1.2 calcium channel in chronic myocardial infarction. *Pflugers Arch* 458:701–711.
4. Liao P, et al. (2007) A smooth muscle Cav1.2 calcium channel splice variant underlies hyperpolarized window current and enhanced state-dependent inhibition by nifedipine. *J Biol Chem* 282:35133–35142.
5. Hofmann F, Flockerzi V, Kahl S, Wegener JW (2014) L-type CaV1.2 calcium channels: From in vitro findings to in vivo function. *Physiol Rev* 94:303–326.
6. Weiss S, Dascal N (2015) Molecular aspects of modulation of L-type calcium channels by protein kinase C. *Curr Mol Pharmacol* 8:43–53.
7. Baudoin C, Goumans MJ, Mummery C, Sonnenberg A (1998) Knockout and knockin of the beta1 exon D define distinct roles for integrin splice variants in heart function and embryonic development. *Genes Dev* 12:1202–1216.
8. Zühlke RD, Bouron A, Soldatov NM, Reuter H (1998) Ca2+ channel sensitivity towards the blocker isradipine is affected by alternative splicing of the human alpha1C subunit gene. *FEBS Lett* 427:220–224.
9. Soong TW, et al. (2002) Systematic identification of splice variants in human P/Q-type channel alpha1(2.1) subunits: Implications for current density and Ca2+-dependent inactivation. *J Neurosci* 22:10142–10152.
10. Maguy A, et al. (2009) Ion channel subunit expression changes in cardiac Purkinje fibers: A potential role in conduction abnormalities associated with congestive heart failure. *Circ Res* 104:1113–1122.
11. Tuluc P, et al. (2009) A CaV1.1 Ca2+ channel splice variant with high conductance and voltage-sensitivity alters EC coupling in developing skeletal muscle. *Biophys J* 96: 35–44.
12. Chen X, et al. (2002) L-type Ca2+ channel density and regulation are altered in failing human ventricular myocytes and recover after support with mechanical assist devices. *Circ Res* 91:517–524.
13. Schröder F, et al. (1998) Increased availability and open probability of single L-type calcium channels from failing compared with nonfailing human ventricle. *Circulation* 98:969–976.
14. Helton TD, Xu W, Lipscombe D (2005) Neuronal L-type calcium channels open quickly and are inhibited slowly. *J Neurosci* 25:10247–10251.
15. Sanguinetti MC, Kass RS (1984) Voltage-dependent block of calcium channel current in the calf cardiac Purkinje fiber by dihydropyridine calcium channel antagonists. *Circ Res* 55:336–348.

16. January CT, Riddle JM (1989) Early afterdepolarizations: Mechanism of induction and block. A role for L-type Ca2+ current. *Circ Res* 64:977–990.
17. Zhang X, Fedida D (1998) Potassium channel-blocking actions of nifedipine: A cause for morbidity at high doses? *Circulation* 97:2098.
18. Antzelevitch C (2004) Cellular basis and mechanism underlying normal and abnormal myocardial repolarization and arrhythmogenesis. *Ann Med* 36:5–14.
19. Nattel S, Maguy A, Le Bouter S, Yeh YH (2007) Arrhythmogenic ion-channel remodeling in the heart: Heart failure, myocardial infarction, and atrial fibrillation. *Physiol Rev* 87:425–456.
20. Madhvani RV, et al. (2011) Shaping a new Ca^{2+} conductance to suppress early afterdepolarizations in cardiac myocytes. *J Physiol* 589:6081–6092.
21. Cherry EM, Hastings HM, Evans SJ (2008) Dynamics of human atrial cell models: Restitution, memory, and intracellular calcium dynamics in single cells. *Prog Biophys Mol Biol* 98:24–37.
22. Maruyama M, et al. (2010) Diastolic intracellular calcium-membrane voltage coupling gain and postshock arrhythmias: Role of purkinje fibers and triggered activity. *Circ Res* 106:399–408.
23. Gellen B, et al. (2008) Conditional FKBP12.6 overexpression in mouse cardiac myocytes prevents triggered ventricular tachycardia through specific alterations in excitation-contraction coupling. *Circulation* 117:1778–1786.
24. Volders PG, et al. (2000) Progress in the understanding of cardiac early afterdepolarizations and torsades de pointes: Time to revise current concepts. *Cardiovasc Res* 46:376–392.
25. Glukhov AV, et al. (2015) Direct evidence for microdomain-specific localization and remodeling of functional L-type calcium channels in rat and human atrial myocytes. *Circulation* 132:2372–2384.
26. Sanchez-Alonso JL, et al. (2016) Microdomain-specific modulation of L-type calcium channels leads to triggered ventricular arrhythmia in heart failure. *Circ Res* 119: 944–955.
27. Bryant SM, et al. (2015) Altered distribution of ICa impairs Ca release at the t-tubules of ventricular myocytes from failing hearts. *J Mol Cell Cardiol* 86:23–31.
28. Groner F, et al. (2004) Single-channel gating and regulation of human L-type calcium channels in cardiomyocytes of transgenic mice. *Biochem Biophys Res Commun* 314: 878–884.
29. Song LS, et al. (2002) Ca(2+) signaling in cardiac myocytes overexpressing the alpha(1) subunit of L-type Ca(2+) channel. *Circ Res* 90:174–181.
30. Muth JN, et al. (1999) Cardiac-specific overexpression of the alpha(1) subunit of the L-type voltage-dependent Ca(2+) channel in transgenic mice. Loss of isoproterenol-induced contraction. *J Biol Chem* 274:21503–21506.
31. Hullin R, et al. (2007) Increased expression of the auxiliary beta(2)-subunit of ventricular L-type Ca(2)+ channels leads to single-channel activity characteristic of heart failure. *PLoS One* 2:e292.
32. Nakayama H, et al. (2007) Ca2+- and mitochondrial-dependent cardiomyocyte necrosis as a primary mediator of heart failure. *J Clin Invest* 117:2431–2444.
33. Beetz N, et al. (2009) Transgenic simulation of human heart failure-like L-type Ca2+-channels: Implications for fibrosis and heart rate in mice. *Cardiovasc Res* 84:396–406.
34. Wheeler DG, Barrett CF, Groth RD, Safa P, Tsien RW (2008) CaMKII locally encodes L-type channel activity to signal to nuclear CREB in excitation-transcription coupling. *J Cell Biol* 183:849–863.
35. Gomez-Ospina N, Tsuruta F, Barreto-Chang O, Hu L, Dolmetsch R (2006) The C terminus of the L-type voltage-gated calcium channel Ca(V)1.2 encodes a transcription factor. *Cell* 127:591–606.
36. Tang ZZ, Zheng S, Nikolic J, Black DL (2009) Developmental control of CaV1.2 L-type calcium channel splicing by Fox proteins. *Mol Cell Biol* 29:4757–4765.
37. Gao C, et al. (2016) RBFox1-mediated RNA splicing regulates cardiac hypertrophy and heart failure. *J Clin Invest* 126:195–206.
38. Fogel BL, et al. (2012) RBFOX1 regulates both splicing and transcriptional networks in human neuronal development. *Hum Mol Genet* 21:4171–4186.
39. Tang M, et al. (2010) Enhanced basal contractility but reduced excitation-contraction coupling efficiency and beta-adrenergic reserve of hearts with increased Cav1.2 activity. *Am J Physiol Heart Circ Physiol* 299:H519–H528.
40. Pan TT, Feng ZN, Lee SW, Moore PK, Bian JS (2006) Endogenous hydrogen sulfide contributes to the cardioprotection by metabolic inhibition preconditioning in the rat ventricular myocytes. *J Mol Cell Cardiol* 40:119–130.
41. Zhang Z, et al. (2005) Functional roles of Cav1.3(alpha1D) calcium channels in atria: Insights gained from gene-targeted null mutant mice. *Circulation* 112:1936–1944.
42. Yue DT, Herzig S, Marban E (1990) Beta-adrenergic stimulation of calcium channels occurs by potentiation of high-activity gating modes. *Proc Natl Acad Sci USA* 87: 753–757.
43. Berul CI, Aronovitz MJ, Wang PJ, Mendelsohn ME (1996) In vivo cardiac electrophysiology studies in the mouse. *Circulation* 94:2641–2648.
44. Wagner S, et al. (2006) Ca2+/calmodulin-dependent protein kinase II regulates cardiac Na+ channels. *J Clin Invest* 116:3127–3138.
45. Cheng H, Lederer WJ, Cannell MB (1993) Calcium sparks: Elementary events underlying excitation-contraction coupling in heart muscle. *Science* 262:740–744.
46. Michele DE, Gomez CA, Hong KE, Westfall MV, Metzger JM (2002) Cardiac dysfunction in hypertrophic cardiomyopathy mutant tropomyosin mice is transgene-dependent, hypertrophy-independent, and improved by beta-blockade. *Circ Res* 91: 255–262.
47. Scherrer-Crosbie M, Thibault HB (2008) Echocardiography in translational research: Of mice and men. *J Am Soc Echocardiogr* 21:1083–1092.
48. Lang RM, et al.; Chamber Quantification Writing Group; American Society of Echocardiography's Guidelines and Standards Committee; European Association of Echocardiography (2005) Recommendations for chamber quantification: A report from the American Society of Echocardiography's Guidelines and Standards Committee and the Chamber Quantification Writing Group, developed in conjunction with the European Association of Echocardiography, a branch of the European Society of Cardiology. *J Am Soc Echocardiogr* 18:1440–1463.
49. Shibata R, et al. (2004) Adiponectin-mediated modulation of hypertrophic signals in the heart. *Nat Med* 10:1384–1389.
50. Lips DJ, et al. (2004) Left ventricular pressure-volume measurements in mice: Comparison of closed-chest versus open-chest approach. *Basic Res Cardiol* 99:351–359.